PROCEEDINGS A

royalsocietypublishing.org/journal/rspa

Research

Cite this article: Silva-Lora A, Torres R. 2020 Explicit Cartesian oval as a superconic surface for stigmatic imaging optical systems with real or virtual source or image. *Proc. R. Soc. A* **476**: 20190894.
http://dx.doi.org/10.1098/rspa.2019.0894

Received: 22 December 2019
Accepted: 3 February 2020

Subject Areas:
optics

Keywords:
cartesian ovals, optical systems, rigorous stigmatism

Author for correspondence:
Rafael Torres
e-mail: rafael.torres@saber.uis.edu.co

Explicit Cartesian oval as a superconic surface for stigmatic imaging optical systems with real or virtual source or image

Alberto Silva-Lora and Rafael Torres

Grupo de Óptica y Tratamiento de Señales, Universidad Industrial de Santander, Bucaramanga, Colombia

AS-L, 0000-0002-1242-5079; RT, 0000-0002-5739-4413

Cartesian ovals, also known as rigorously stigmatic surfaces, are the simplest optical systems capable of producing a perfect point image. Exist both implicit and explicit expressions to represent these surfaces, but they treat both refractive and reflective surfaces independently. Because of the complexity of explicit expressions, the ray-tracing techniques for these surfaces are implemented using third-party software. In this paper, we express Cartesian ovals as a degenerated superconic curve and get a new explicit formulation for Cartesian ovals capable of treating image formation using both object and image points, either real or virtual, and in this formulation can deal with both reflective and refractive rigorously stigmatic surfaces. Finally, using the resultant expressions and the vector Snell–Descartes Law, we propose a self-contained analytical ray-tracing technique for all these surfaces.

1. Introduction

The theory of rigorous stigmatism studies the surfaces suitable for perfect point image formation from a point object. Those points are known as rigorously stigmatic points [1] and the surfaces capable of imaging a perfect point are known as *Rigorously Stigmatic Surfaces* (RSS). These surfaces were stated firstly by Descartes [2] and then studied by Huygens [3]. They are also known as Cartesian ovals, widely studied for many authors [4–6], including the case for a negative index of refraction [7]. As particular cases of RSS, we can find the conics of revolutions that include the spherical refracting surface

THE ROYAL SOCIETY PUBLISHING

and the plane surface, which form an aberration-free image on its rigorously stigmatic points [8,9]. These particular cases are of special interest and are applied in different areas such as microscopy [10], astronomy [11] and machine vision [12], but recently it has been evidenced a practical interest in the Cartesian ovals and aspherical surfaces. Not limited to their applications, we find works as the design of catadioptric systems [13], the design of compound refractive lens systems (CRL) to focus X-rays [14,15], Cartesian ovals representations for illumination systems [16], the design of a immersion lens [17] and the manufacture of a high-resolution system to polish corrective optical surfaces with or without rotational symmetry [18]. In general, optical imaging systems are built using spherical surfaces, due to these surfaces being simpler to polish [19] and because they also present rigorously stigmatic points known as Young–Weierstrass points [20–22].

Spherical surfaces can produce aberration-free images from point objects located on its rigorously stigmatic points. If a point object lies in a different location than the rigorously stigmatic points, the imaging system will no longer produce a perfect point image, and the geometry of the imaging system will induce spherical aberration on it. The spherical aberration emerges because all refracted rays, starting from a point object located at a different point than rigorously stigmatic points, match at different points on the optical axis.

Aberrations can be minimized using different methods, a method is to use compensating surfaces that allows correcting the distortion produced on the image. There are a variety of corrective surfaces mentioned in the literature, such as standard aspherical surfaces [23], subconic surfaces, superconic surfaces [24] and free-form surfaces [25,26], among others. The formulation presented in [25] correct spherical aberrations just when both object and image are real and the magnification is negative. Additionally, the author refers to 'general Cartesian problem' to find a surface that transforms a given incident wavefront into another given wavefront, but how we have mentioned here, Cartesian Ovals transform a spherical wavefront into another spherical wavefront. Superconic surfaces have certain advantages over standard aspherical surfaces, due to superconic surfaces can represent better highly sloped surfaces with fewer high-order aspheric terms, in some cases obtaining better results. Due to this, superconic surfaces are more stable in optimization processes [24]. Cho *et al*. [27] shows an explicit formulation of another type of superconic surfaces, where not only conics and Cartesian ovals are particular cases but also standard aspherical surfaces. Superconics are used as corrective surfaces that compensate aberrations in optical imaging systems as do the standard aspherical surfaces [24].

Usually, RSS are represented using an implicit expression, but in optics, an explicit formulation of these surfaces is of greater interest [28]. Explicit formulations of these surfaces provide advantages in the optical design area, including the production of lenses and mirrors. It is important to mention that an explicit formulation is also helpful in computer-aided design and computer-aided manufacturing processes, providing the necessary tools to define an error function [18,29]. Additionally, we believe that an explicit expression could be used to design methods to formulate corrective surfaces that compensate aberrations in optical systems composed by RSS, when point object does not lie at the rigorously stigmatic point. Several works have addressed the explicit formulation of an RSS, based on Ferrari's method [30], both exactly [15,31–33] or approximated, using series expansion [32] or using aspherical surfaces [34], some of them listed in table 1. The exact mathematical expression of RSS are emphasized in a real point image formation using a real point object, but the cases for virtual object or image have not received the same attention, but in [15], not limited to this configuration, are applied Cartesian surfaces to virtual point objects. Due to the complexity of exact expressions for this kind of optical surfaces, the authors make use of third-party software as *OSLO* [34,37] to carry out the ray tracing. It is worth to mention that a formulation for ray tracing through funnel concentrator optics as toroids generated from parabolic and elliptical surfaces was proposed [38].

Most published explicit expressions of Cartesian ovals are obtained using the Ferrari's method [30], where the general quartic equation is transformed by a change of variable into a depressed quartic equation, to then introduce an arbitrary variable that leads to obtaining the roots of a cubic equation. In all these works, the results are formulated through various formulae that

Table 1. Comparative table of works associated with methods to produce aspherical surfaces in the area of optical science, and related to explicit and implicit expressions to characterize Cartesian oval.

author	kind of expression	characteristics
Chun-Che Hsueh [31]	explicit, exact	Explicit formulation of Cartesian ovals obtained by Ferrari's method.
Juan Camilo Valencia-Estrada [35]	explicit, exact	Patent related with the design of lenses composed of aspherical oval surfaces.
Juan Camilo Valencia-Estrada [32]	explicit, exact	Explicit formulation of Cartesian ovals from the solution of a nonlinear and the first-order differential equation. Explicit solution by using the Fermat principle.
Cristian E. Gutierrez [36]	explicit, exact	Explicit formulation of Cartesian ovals written in polar coordinates. The solution is obtained by solving a quartic equation, but the authors just cover the case for real object and real image.
Sunggoo Cho [27]	explicit, exact	Development of an explicit expression used to characterize Cartesian ovals that correspond to an optical solution.
Juan Camilo Valencia-Estrada [34]	explicit, approximated	Computation of asphericity coefficients to fit aspherical surfaces with Cartesian ovals surfaces.

allow representing the ovoids of Descartes as compound curves. In this work, taking advantage of the implicit expression of the Cartesian ovals as a particular case of superconic surfaces, are characterized the RSS as an exact explicit expression using polar parameters on the meridional plane, by solving a cubic equation. Employing these expressions are build the necessary tools for the analytical formulation of the ray tracing. As a result of this work, we provide a single unified equation for ideally focusing refracting and reflecting surfaces, with both object and image either real or virtual. Using this equation, we show that these surfaces are degenerate forms of superconic surfaces that, as we mentioned above, present some advantages over the standard aspherical surfaces when representing highly sloped surfaces [24]. We believe that the treatment of Cartesian ovals as a particular case of superconic surfaces is advantageous when correcting lenses with a large aperture, which is analogous to have highly sloped surfaces.

The implicit expression of the RSS and its relation with conic and aspherical surfaces is shown in §2. These surfaces as a particular case of a superconic surface are represented in §3. This representation is crucial to define a series of shape parameters employed to obtain an explicit formulation of the RSS. The result is expressed using polar parameters on the meridional plane. In §4, both implicit and explicit expressions are used to establish the fundamental mathematical components to implement ray tracing through RSS characterized by Cartesian ovals. Some computational results for general and particular cases of RSS obtained adopting this formulation are shown in §5.

2. Implicit formulation of the RSS

Considering a spherical refracting surface within the paraxial approximation, the image of a spherical wavefront object field tangent to the refracting surface is another spherical wavefront also tangent to the refracting surface whose centres of curvature are paraxial images of each other. In a more general sense, we define *the aplanatic image of a tangent incident spherical wavefront to a Cartesian oval*:

Definition 2.1. A rigorously stigmatic system is such a system able to transform a spherical wavefront $\mathcal{A}$ into another spherical wavefront $\mathcal{A}'$, whose centres of curvature A and A', are the

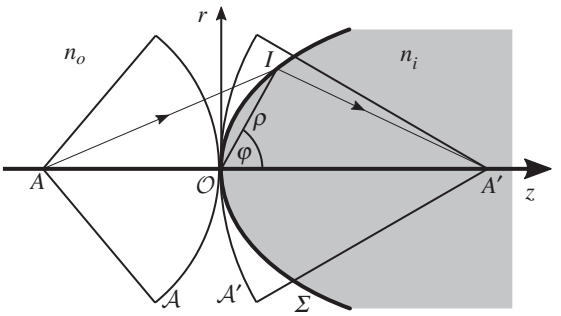

Figure 1. The surface, represented by Σ, transforms the incident spherical wave wavefront $\mathcal{A}$ into an emergent spherical wave wavefront $\mathcal{A}'$.

rigorously stigmatic points (figure 1). Thus, the spherical wavefront $\mathcal{A}'$ is the aplanatic image of the spherical wavefront $\mathcal{A}$.

According to figure 1, surfaces identified by letter Σ that meet the rigorous stigmatism theory and therefore satisfy definition 2.1, are expressed as follows:

$$n_o|\boldsymbol{\rho} - \boldsymbol{\xi}_o| + n_i|\boldsymbol{\rho} - \boldsymbol{\xi}_i| = k. \tag{2.1}$$

Expression (2.1) is known as Fermat's equation, where $\boldsymbol{\xi}_o = (0, 0, z_o)$ is the position of the point object A, $\boldsymbol{\xi}_i = (0, 0, z_i)$ is the position of the point image A', $\boldsymbol{\rho} = (x, y, z)$ is a vector that determines a point on the Σ surface, and k is an arbitrary constant.

Remark 2.2 (Sign convention). Unless otherwise stated, light is assumed to propagate from left to right. We have adopted the following sign convection:

— Distances are considered algebraic quantities determined from position $\mathcal{O}$.
— Distances with the direction of light propagation are considered positive otherwise negative.

Holding Fermat sign's rule, established in remark 2.2, we consider the object distance, $z_o = \overline{\mathcal{O}A}$, as an algebraically negative quantity and the image distance, $z_i = \overline{\mathcal{O}A'}$, a positive one. According to this and considering that the surface Σ passes through the origin of coordinates, $\mathcal{O}$, we take $k = n_i z_i - n_o z_o$, and thus expression (2.1) is written as follows:

$$n_o\sqrt{x^2 + y^2 + (z - z_o)^2} + n_i\sqrt{x^2 + y^2 + (z - z_i)^2} = n_i z_i - n_o z_o, \tag{2.2}$$

where the length $|z_o| = \sqrt{z_o^2} = -z_o$. By squaring both sides of expression (2.2) to eliminate the radical, is obtained

$$\begin{aligned}&\left[(n_i^2 - n_o^2)(x^2 + y^2 + z^2) - 2z(n_i^2 z_i - n_o^2 z_o)\right]^2 \\ &\quad - 4n_i n_o(n_i z_i - n_o z_o)\left[(n_o z_i - n_i z_o)(x^2 + y^2 + z^2) + 2z_i z_o(n_i - n_o)z\right] = 0,\end{aligned} \tag{2.3}$$

which is an implicit expression of a Cartesian oval, where the points A and A' are known as rigorously stigmatic points.

(a) Object or image at infinity

Equation (2.3) is a general expression but certain particular cases of Cartesian ovals have an especial interest in optics, one of these cases is obtained when the point object lies at infinity,

$z_o \to -\infty$, for which equation (2.3) is reduced to

$$\left[z - \frac{n_i z_i}{n_o + n_i}\right]^2 + \left[\frac{n_i^2}{n_i^2 - n_o^2}\right](x^2 + y^2) = \left[\frac{n_i z_i}{n_i + n_o}\right]^2, \tag{2.4}$$

if $n_i > n_o$ the surface is an ellipsoid and if $n_i < n_o$ is a hyperboloid.

(b) Spherical refracting surface

Another relevant case results if is taken $z_o = n_i/\kappa$ and $z_i = n_o/\kappa$, where κ is an arbitrary constant. Substituting z_o and z_i values into equation (2.3) is obtained a sphere, written as

$$(x^2 + y^2) + \left[z - \frac{n_o n_i}{\kappa(n_o + n_i)}\right]^2 = \left[\frac{n_o n_i}{\kappa(n_o + n_i)}\right]^2, \tag{2.5}$$

where $R = n_o n_i[\kappa(n_o + n_i)]^{-1}$ is the radius of the sphere and points z_o and z_i are known as Young–Weierstrass' points [20] which correspond to the rigorously stigmatic points of a spherical refracting surface, which are expressed as function of the radius of the sphere by

$$z_o = \frac{R(n_o + n_i)}{n_o} \tag{2.6}$$

and

$$z_i = \frac{R(n_o + n_i)}{n_i}. \tag{2.7}$$

Spherical refracting surfaces present infinite rigorously stigmatic points which also form spherical surfaces known as aplanatic surfaces [39] fulfilling the Abbe sine condition [40].

(c) Reflecting RSS

Reflective surfaces are important components in the optical imaging systems manufacturing such as telescopes. This kind of components provides certain advantages over refractive surfaces, such as shorter devices and zero chromatic aberrations.

Usually, reflective surfaces are managed independently from refractive surfaces. In the formulation presented here, the reflective rigorously stigmatic surfaces are obtained using the same formulation by making $n_i = -n_o$, which reduces the Cartesian oval expression to a conic surface, expressed as:

$$\left[z - \frac{z_o + z_i}{2}\right]^2 + \left[\frac{(z_i + z_o)^2}{4 z_i z_o}\right](x^2 + y^2) = \left[\frac{z_i + z_o}{2}\right]^2. \tag{2.8}$$

If $z_i z_o > 0$, this surface matches an ellipsoid and if $z_i z_o < 0$ it matches a hyperboloid.

It can also be observed from equation (2.8) that if $z_o \to -\infty$ the equation is reduced to

$$4 z_i z - (x^2 + y^2) = 0, \tag{2.9}$$

which is a paraboloidal surface. For $z_i > 0$ the paraboloidal surface opens toward the positive side of the z-axis and if $z_i < 0$ it opens towards the negative side.

(d) Relationship of RSS with standard aspherical surfaces

As we have seen, conics are particular cases of Cartesian ovals. Consequently, these surfaces present rigorous stigmatism [41]. An explicit expression for conics surfaces is

$$z = \frac{c_0' r^2}{1 + \sqrt{1 - (1 + K') c_0'^2 r^2}}, \tag{2.10}$$

known as Schwarzschild equation [42], where $K' = -e^2$ (e being the eccentricity) is the Schwarzschild constant, c_0' is the curvature and $r^2 = x^2 + y^2$.

When the point object does not match the conic rigorously stigmatic point aberrations emerge, distorting the image. These distortions are characteristic of the optical surface geometry and traditionally these are mentioned as spherical aberrations due to spherical surfaces are the most used. Nevertheless, for each surface (spherical, hyperboloidal, ellipsoidal and paraboloidal), aberrations are presented in a particular form [21], including both reflective and refractive surfaces. Hence, to minimize the effect of aberrations on the image, additional higher-order terms are added to equation (2.10). These terms are called deformation terms, which allow generating new surfaces corresponding to deformed versions of conics that belong to the family of aspherical surfaces.

So, standard aspherical surfaces are formulated as follows [23]:

$$z = \frac{c_0' r^2}{1 + \sqrt{1 - (1 + K')c_0'^2 r^2}} + \sum_{j=2} A_{2j} r^{2j}, \tag{2.11}$$

where coefficients A_{2j} are called asphericity coefficients. Thus, conics surfaces can also be viewed as degenerated cases of the standard aspherical surfaces. Surfaces given by equation (2.11) are not equivalent to Cartesian ovals and they are not RSS except for the cases when $A_{2j} = 0$. The asphericity coefficients can be adapted to minimize aberrations, and thus these aspherical surfaces are used to compensate an aberrated wavefront [23]. Taking advantage of this property from aspherical surfaces, are build isoplanatic optical systems [28]. Correcting an aberrated wavefront using equation (2.11), is carried out finding appropriated asphericity coefficients according to the order of the aberrations to be minimized or eliminated. Additionally, these aspheric surfaces are used as approximated stigmatic surfaces, forming an approximated stigmatic image [34].

Recently, there have been improvements around subjects related to minimization of optical aberrations using aspheric lenses, and subjects related to Cartesian ovals. In table 1, we show information about these types of progress. Some authors have achieved to express Cartesian ovals implicitly and explicitly but considering refractive and reflective optical surfaces separately. These expressions handle a minimum of two solutions.

In the following section, based on the relation between another kind of corrective surfaces known as superconic surfaces, we deduce an explicit expression of Cartesian ovals. This expression characterizes surfaces free of all orders of spherical aberration in a novel way, for point object and image on the optical axis.

3. Explicit expression of Cartesian ovals

Although applications using Cartesian ovals as optical surfaces seem restricted, since these surfaces have just a pair of stigmatic points (except for spherical refracting surfaces on aplanatic surfaces), are these surfaces the key to understand the basics of designing systems with a minimum of optical aberrations.

An almost standard methodology to correct the effect of aberrations on the image formation is to formulate RSS as a particular case of other ones, capable of being adapted to eliminate or minimize these aberrations, and so achieving an approximately stigmatic image [34]. As we mentioned before, standard aspherical surfaces are written as deformed conics surfaces and are used to correct aberrations. In addition to aspherical surfaces, there is another type of corrective surfaces, known as superconics surfaces [24] and are written as deformed Cartesian ovals.

All these types of surfaces are applied to fabricate optical elements like lenses and mirrors. These elements, in turn, are used in the optical design field to improve the design and image quality of optical imaging systems. An advantage of superconics over standard aspherical surfaces is that superconics can achieve better results minimizing aberrations presented in optical imaging systems due to being able to better represent steep surfaces using fewer aspheric terms than the standard aspheric surfaces [24].

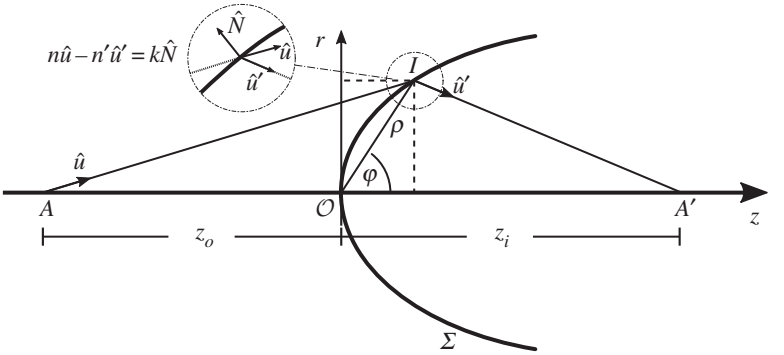

Figure 2. Rigorously stigmatic quartic surface.

(a) Cartesian ovals as superconics

Restructuring expression (2.3), we obtain an expression of Cartesian ovals written as a degenerated superconic surface. Then by taking $\rho^2 = x^2 + y^2 + z^2$, we have

$$4\left(n_i^2 z_i - n_o^2 z_o\right)^2 z^2 - 2\left[4n_i n_o z_i z_o\,(n_i - n_o)\,(n_i z_i - n_o z_o) + 2\,(n_i - n_o)\,(n_i + n_o)\,(n_i^2 z_i - n_o^2 z_o)\rho^2\right]z + \left[4n_i n_o\,(n_i z_i - n_o z_o)\,(n_i z_o - n_o z_i) + (n_i - n_o)^2\,(n_i + n_o)^2\,\rho^2\right]\rho^2 = 0, \tag{3.1}$$

dividing by

$$D = 4n_i n_o z_i z_o\,(n_i - n_o)\,(n_i z_i - n_o z_o)\,, \tag{3.2}$$

and defining the following parameters:

$$K = \frac{\left(n_i^2 z_i - n_o^2 z_o\right)^2}{n_i n_o\,(n_i z_i - n_o z_o)\,(n_i z_o - n_o z_i)}, \tag{3.3}$$

$$c_0 = \frac{n_i z_o - n_o z_i}{z_i z_o\,(n_i - n_o)}, \tag{3.4}$$

$$c_1 = \frac{(n_i - n_o)\,(n_i + n_o)^2}{4n_i n_o z_i z_o\,(n_i z_i - n_o z_o)} \tag{3.5}$$

and

$$b_1 = \frac{(n_i + n_o)\left(n_i^2 z_i - n_o^2 z_o\right)}{2n_i n_o z_i z_o\,(n_i z_i - n_o z_o)}, \tag{3.6}$$

called shape parameters, then we can express Cartesian ovals as follows:

$$c_0 K z^2 - 2(1 + b_1\rho^2)z + (c_0 + c_1\rho^2)\rho^2 = 0. \tag{3.7}$$

Thus, the Cartesian ovals appear as degeneration of superconic surfaces defined in [24] as

$$c_0 K z^2 - 2(1 + b_1\rho^2 + b_2\rho^4 + \cdots)z + (c_0 + c_1\rho^2 + c_2\rho^4 + \cdots)\rho^2 = 0, \tag{3.8}$$

where K and c_0 are analogous to Schwarzschild constant and curvature, respectively, in the case of conic surfaces.

(b) Explicit expression for Cartesian ovals

From this association, we develop a closed-form expression for Cartesian ovals, this expression is formulated using the polar parameters ρ and φ on the meridional plane as shown in figure 2.

Considering $z \equiv \rho \cos\varphi$, we can reduce the expression (3.7) into a third-order polynomial in ρ, written as follows:

$$a\rho^3 + b\rho^2 + c\rho + d = 0, \tag{3.9}$$

where

$$a = c_1, \tag{3.10}$$

$$b = -2b_1 \cos\varphi, \tag{3.11}$$

$$c = c_0(K\cos^2\varphi + 1) \tag{3.12}$$

and

$$d = -2\cos\varphi. \tag{3.13}$$

According to Cardano's method [43], the solutions for (3.9) are expressed as

$$\rho_1 = S + T - \frac{b}{3a}, \tag{3.14}$$

$$\rho_2 = -\frac{S+T}{2} - \frac{b}{3a} + \mathrm{i}\sqrt{3}\frac{S-T}{2} \tag{3.15}$$

and

$$\rho_3 = -\frac{S+T}{2} - \frac{b}{3a} - \mathrm{i}\sqrt{3}\frac{S-T}{2}, \tag{3.16}$$

where

$$S = \left(R + \sqrt{Q^3 + R^2}\right)^{1/3}, \tag{3.17}$$

$$T = \left(R - \sqrt{Q^3 + R^2}\right)^{1/3} \tag{3.18}$$

and

$$Q = \frac{3ac - b^2}{9a^2}, \tag{3.19}$$

$$R = \frac{9abc - 27a^2d - 2b^3}{54a^3}. \tag{3.20}$$

Using the three solutions obtained by Cardanos's method, identified by equations (3.14)–(3.16), we get the values of coordinates r and z, as follows:

$$r = \rho_i \sin\varphi \tag{3.21}$$

and

$$z = \rho_i \cos\varphi, \tag{3.22}$$

with $i = 1, 2, 3$. Applying equations (3.21) and (3.22), we can generate a set of Cartesian ovals for different position of object and image, as is shown in figure 3. Cartesian surfaces are curves that have three focus, where two of them are the object position (z_o) and the image position (z_i), being these two points conjugate stigmatic points for the surface that passes through the origin of coordinates. We can see that solutions ρ_1 and ρ_2 result in the same curves that do not pass through the origin of coordinates. We are not interested in these solutions, because of the acceptable optically solution that satisfies the condition $k = n_i z_i - n_o z_o$ (2.2) must pass by the origin. Conversely, solution ρ_3 passes through the origin of coordinates, so this is the solution to consider, thus, we take $\rho = \rho_3$. The solution with a physical interest is that one with real values for $\rho(\varphi)$. The values of $\rho(\varphi)$ are real if $Q^3 + R^2 < 0$, then $S + T$ is real and $S - T$ is a pure imaginary value, this leads to solution (3.16) being real.

Finally, the explicit expression for the RSS can be written if (3.10)–(3.13) are substituted into equations (3.19) and (3.20), to later substitute the result obtained into expressions (3.17) and (3.18),

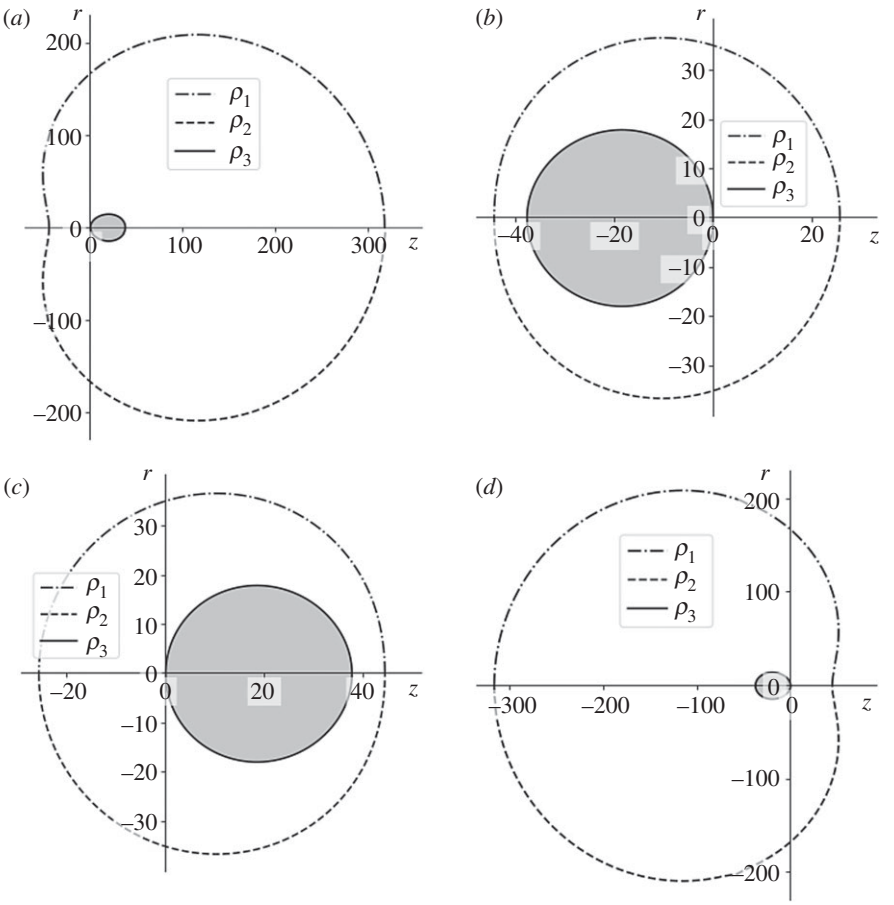

Figure 3. Graphical result of surface $\rho(\varphi)$ on the meridional plane (r, z), when varying object and image positions. (*a*) $z_o < 0$ and $z_i > 0$. (*b*) $z_o < 0$ and $z_i < 0$. (*c*) $z_o > 0$ and $z_i > 0$. (*d*) $z_o > 0$ and $z_i < 0$. For all the cases $n_i > n_o$.

to finally substitute this result into equation (3.16). Considering that $b_1^2 - c_0 c_1 K = 0$, we can write ρ as a function of φ as follows:

$$\rho = -\left(A_1 \cos(\varphi) + A_3 \cos^3(\varphi) - \sqrt{A_0 + A_2 \cos^2(\varphi) + A_4 \cos^4(\varphi)}\right)^{1/3} e^{-i\pi/3}$$
$$- \left(A_1 \cos(\varphi) + A_3 \cos^3(\varphi) + \sqrt{A_0 + A_2 \cos^2(\varphi) + A_4 \cos^4(\varphi)}\right)^{1/3} e^{i\pi/3} + \frac{2b_1 \cos(\varphi)}{3c_1}, \quad (3.23)$$

where

$$A_0 = \frac{K^3 c_0^6}{27 b_1^6}, \quad (3.24)$$

$$A_1 = -\frac{K c_0 \left(K c_0^2 - 3 b_1\right)}{3 b_1^3}, \quad (3.25)$$

$$A_2 = \frac{K^2 c_0^2 \left(2K^2 c_0^4 - 18 K b_1 c_0^2 + 27 b_1^2\right)}{27 b_1^6}, \quad (3.26)$$

$$A_3 = -\frac{K^3 c_0^3}{27 b_1^3} \tag{3.27}$$

and

$$A_4 = \frac{K^4 c_0^4 \left(K c_0^2 - 2 b_1\right)}{27 b_1^6}. \tag{3.28}$$

Through equation (3.23), we can compute any point (z, r) on the surface given by

$$z(\varphi) = \rho(\varphi)\cos(\varphi) \tag{3.29}$$

and

$$r(\varphi) = \rho(\varphi)\sin(\varphi). \tag{3.30}$$

And these equations characterize in general form the Cartesian ovals that represent RSS.

Equation (3.23) is our main result, which allows us to obtain the solution of rigorously stigmatic surfaces. With this formulation, we can consider different configurations of rigorously stigmatic points, objects, and images, either real or virtual. When the object position is less than zero ($z_o < 0$), the object is real otherwise it is virtual, and when the image position is greater than zero ($z_i > 0$), the image is real otherwise it is virtual. These results constitute an advantage since using a single equation are obtained different RSS for different configurations of the object and image.

From the results obtained in equations (3.7) and (3.23), along with expressions (3.29) and (3.30), we can think about a strategy to develop analytical expressions for ray-tracing. This formulation is used to visualize ray paths from the point object to the point image, thus corroborating the stigmatic image formation through an optical surface characterized by a Cartesian oval. This is addressed in the next section adopting the vector Snell–Descartes' law.

4. Analytical ray-tracing through Cartesian ovals

We developed an analytical method for ray-tracing through Cartesian ovals, obtained using the Snell–Descartes vector law. We began by finding an unit normal vector to Cartesian oval surfaces $\rho(\varphi)$ defined in equation (3.23).

Given a rigorously stigmatic surface $\rho(z(\varphi), r(\varphi))$, we can define the parametrized surface as

$$\boldsymbol{\rho} = \begin{bmatrix} z(\varphi) \\ r(\varphi) \end{bmatrix}, \tag{4.1}$$

from which we obtain the tangent vector to this surface, denoted by

$$\boldsymbol{T} = \begin{bmatrix} \dfrac{\mathrm{d}z(\varphi)}{\mathrm{d}\varphi} \\ \dfrac{\mathrm{d}r(\varphi)}{\mathrm{d}\varphi} \end{bmatrix}. \tag{4.2}$$

Thus, the normal vector to the Cartesian ovals is

$$\boldsymbol{N} = \begin{bmatrix} -\dfrac{\mathrm{d}r(\varphi)}{\mathrm{d}\varphi} \\ \dfrac{\mathrm{d}z(\varphi)}{\mathrm{d}\varphi} \end{bmatrix}. \tag{4.3}$$

It is this normal vector $\boldsymbol{N}$ that determines according to Snell–Descartes vector law the direction $\hat{u}'$ taken by the refracted ray for a given direction $\hat{u}$ of the incident ray (figure 2).

Considering the above definitions, and using expressions (3.29) and (3.30), we formulate the unit normal vector as follows:

$$\widehat{N} = \frac{-(\mathrm{d}r/\mathrm{d}\varphi)\,\hat{z} + (\mathrm{d}z/\mathrm{d}\varphi)\,\hat{r}}{\sqrt{(\mathrm{d}r/\mathrm{d}\varphi)^2 + (\mathrm{d}z/\mathrm{d}\varphi)^2}}, \tag{4.4}$$

and using equations (3.29) and (3.30), we get

$$\frac{\mathrm{d}z}{\mathrm{d}\varphi} = \frac{\mathrm{d}\rho}{\mathrm{d}\varphi}\cos\varphi - \rho\sin\varphi \tag{4.5}$$

and

$$\frac{\mathrm{d}r}{\mathrm{d}\varphi} = \frac{\mathrm{d}\rho}{\mathrm{d}\varphi}\sin\varphi + \rho\cos\varphi, \tag{4.6}$$

where ρ is given by equation (3.9), then

$$\frac{\mathrm{d}\rho}{\mathrm{d}\varphi} = \frac{-2(b_1\rho^2 - c_0K\rho\cos\varphi + 1)\sin\varphi}{3c_1\rho^2 - 4b_1\rho\cos\varphi + c_0(K\cos^2\varphi + 1)}. \tag{4.7}$$

Hence, substituting expressions (4.6) and (4.5) into equation (4.4), we get that the unit normal vector to Cartesian ovals surfaces, is written as

$$\widehat{N} = \frac{-\left((\mathrm{d}\rho/\mathrm{d}\varphi)\sin\varphi + \rho\cos\varphi\right)\hat{z} + \left((\mathrm{d}\rho/\mathrm{d}\varphi)\cos\varphi - \rho\sin\varphi\right)\hat{r}}{\left[(\mathrm{d}\rho/\mathrm{d}\varphi)^2 + \rho^2\right]^{1/2}}, \tag{4.8}$$

with $\mathrm{d}\rho/\mathrm{d}\varphi$ given by (4.7).

Using equations (3.29) and (3.30), we can also define the unit vector of the incident ray. This is defined as the difference between the position vector of a point on the rigorously stigmatic surface, defined by the vector equation (4.1), and the vector $\boldsymbol{d} = [z_o, 0]$ pointing the point object, divided by the magnitude of the resultant vector. Thus, the unit vector of the incident ray is expressed by

$$\hat{u} = \frac{(\rho\cos\varphi - z_o)\,\hat{z} + \rho\sin\varphi\hat{r}}{\sqrt{\rho^2 + z_o^2 - 2z_o\rho\cos\varphi}}. \tag{4.9}$$

Finally, using equations (4.8) and (4.9), and the Snell–Descartes vector law [44], the unit vector of the refracted ray is written as

$$\hat{u}' = \tau\hat{u} - \left(\tau(\widehat{N}\cdot\hat{u}) + \sqrt{1 - \tau^2\left(1 - (\widehat{N}\cdot\hat{u})^2\right)}\right)\widehat{N}, \tag{4.10}$$

where $\tau = n_o/n_i$. The two-dimensional equation (4.10) can be easily transformed into a three-dimensional one as is done in [29]. Expressions (4.8)–(4.10) allow the ray-tracing through Cartesian ovals surfaces in an analytic form, thus calculate accurately the path of a bunch of rays through RSS represented by expression (3.23). This can be applied to study aberrations when the point object does not lie on aplanatic points.

In the following section, we show some results and examples of RSS obtained using the explicit expression (3.23). These results include both refractive and reflective surfaces. They also include points object and image, either real or virtual.

5. Computational results using explicit expression

Ray-tracing is the most used method by optical designers to study the performance of optical imaging systems. As a starting point, we have derived a method for exact ray tracing through a rigorously stigmatic surface. This method allows us to calculate the ray paths to reach the image after being refracted or reflected by these types of surfaces.

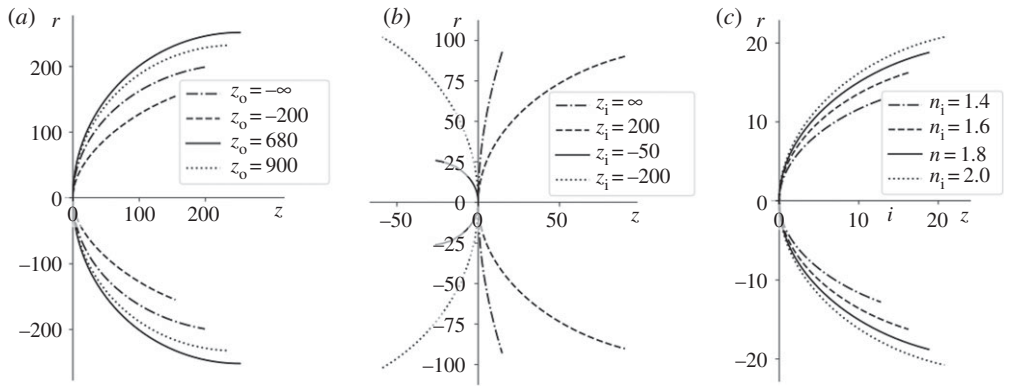

Figure 4. Graphical representation of RSS. Object and image distances are finite quantities. (*a*) Variations of object distance z_o. (*b*) Variations of image distance z_i. (*c*) Variations of the index of refraction of image space n_i.

(a) Refractive surface

Considering expression (3.23) and substituting into expressions (3.29) and (3.30), we characterize Cartesian ovals surfaces. We study perfect image formation through a refracting surface described by these RSS using ray-tracing method constituted by equations (4.8)–(4.10). Here is shown how the shape of a refracting optical surface characterized by RSS is changed, first, when object or image position is changed, and then for different refractive indexes of the media. For each variation of these quantities a different optical surface is obtained. This is important in the process of optimization of optical systems to obtain the configuration to achieve the best performance.

When the object point or the image point is situated at the infinite the parameters b_1 and c_1 vanish and equation (3.7) reduces to

$$(K+1)c_0z^2 - 2z + c_0r^2 = 0, \tag{5.1}$$

also represented by

$$\left[z - \frac{1}{(K+1)c_0}\right]^2 + \frac{r^2}{K+1} = \frac{1}{(K+1)^2c_0^2}, \tag{5.2}$$

which corresponds to a conical of revolution.

(i) Ellipsoids

Expression (5.2) is a degenerated Cartesian oval and becomes to ellipsoidal surface when $K+1 > 0$ and the value of K, equation (3.3), reduces to

$$K = -\left(\frac{n_o}{n_i}\right)^2, \tag{5.3}$$

and $K+1 > 0$ if $n_i > n_o$.

Figure 4*a* shows different RSS after varying object distance z_o and keeping fixed values of $n_o = 1$, $n_i = 1.7$, and $z_i = 400$. When the value of z_o lies at infinity, the surface is ellipsoidal.

(ii) Hyperboloids

Another case of degenerated Cartesian oval, represented by expression (5.2), is obtained for $K+1 < 0$ and the value of K, equation (3.3), reduces to

$$K = -\left(\frac{n_i}{n_o}\right)^2, \tag{5.4}$$

and $K+1 < 0$ if $n_i > n_o$.

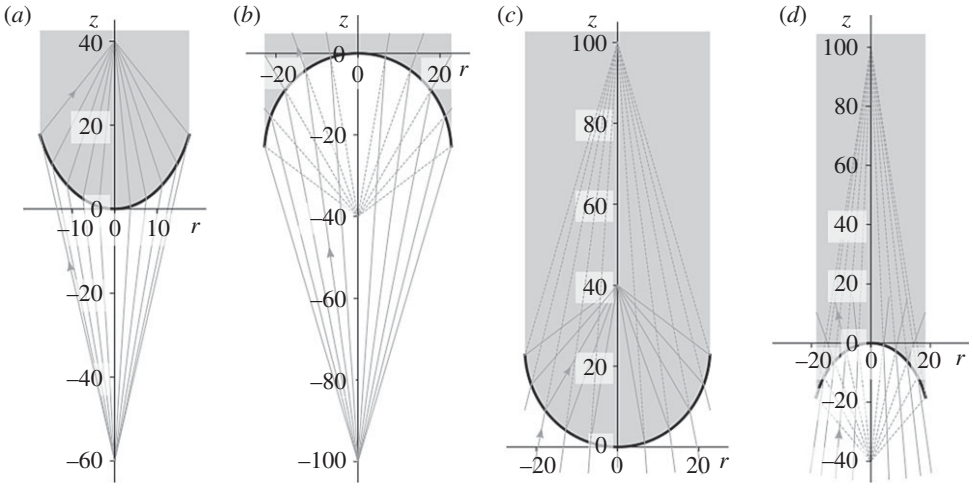

Figure 5. Exact ray tracing through RSS. (*a*) Real point object placed at $z_o = -60$ and real point image placed at $z_i = 40$. (*b*) Real point object placed at $z_o = -100$ and virtual point image placed at $z_i = -40$. (*c*) Virtual point object placed at $z_o = 100$ and real point image placed at $z_i = 40$. (*d*) Virtual point object placed at $z_o = 100$ and virtual point image placed at $z_i = -40$. The indexes of refraction of the media are $n_o = 1.0$, for object space, and $n_i = 1.7$, for image space.

Varying image position z_i and taking fixed values of $n_o = 1$, $n_i = 1.7$, and $z_o = -400$, we show in figure 4*b* different cases of RSS for different values of z_i including the limited case when z_i lies at the infinite, which corresponds to a hyperboloidal surface.

The degenerated RSS, together with non-degenerated RSS, can be used to design more complex optical systems as a photographic lens system. The advantage is that all the RSS represented here are rigorously stigmatic at the rigorously stigmatic points on the optical axis.

(iii) Cartesian ovals for different refractive index

As we can observe in figure 4*c*, it is shown some curves varying index of refraction, n_i, of the image space, and keeping fixed values of $n_o = 1$, $z_o = -60$, and $z_i = 40$. So, we observe there how the curve is wider as the refractive index increases.

The RSS change in shape for different values of the parameters they depend on. For different values of the refractive indexes, there are different surfaces for the same aplanatic points. The variation of these parameters is the key to the optimization processes carried out to design isoplanatic optical systems [45].

(iv) Discussion about simulation results

In this section, we present some computational results of RSS performance, by using our ray-tracing technique and the explicit expression (3.23), for different settings of object and image location.

Some computational results for Cartesian ovals are shown in figure 5. Figure 5*a* shows a perfect real image formation from a real point object, figure 5*b* shows a perfect virtual image formation from a real point object, figure 5*c* shows a perfect real image formation from a virtual point object and figure 5*d* shows a perfect virtual image formation from a virtual point object. Using the ray-tracing method represented by equations (4.8)–(4.10), we check the performance for these RSS.

According to the results presented here, we announced in a general form that a rigorously stigmatic surface can transform perfectly an incident spherical wavefront into another spherical wavefront, as shown in figure 6. The coherent image of a spherical surface $\mathcal{A}$ centred at A and tangent to refracting surface $\mathcal{D}$, is another sphere $\mathcal{A}'$ centred at A' and also tangent to refracting

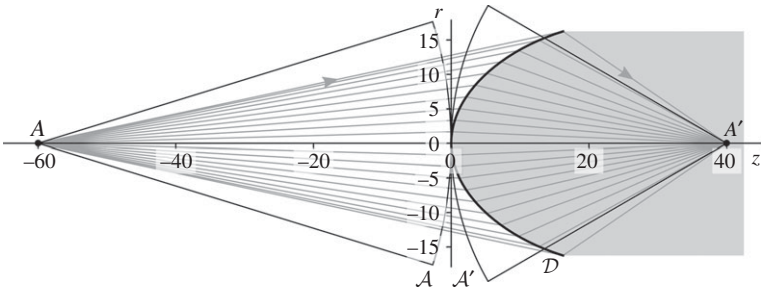

Figure 6. Transformation of the spherical wavefront, $\mathcal{A}$, into another spherical wavefront, $\mathcal{A}'$, through a refracting surface $\mathcal{D}$ represented by a rigorously stigmatic surface.

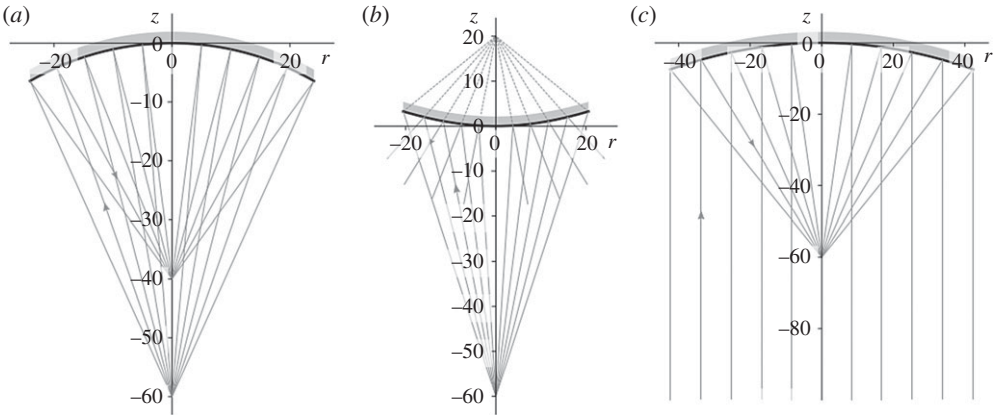

Figure 7. Exact ray-tracing through RSS for a perfect image formation. (*a*) Ellipsoidal mirror with real point object placed at $z_o = -60$ and real image at $z_i = -40$. (*b*) Hyperboloidal mirror with real point object placed at $z_o = -60$ and virtual image at $z_i = 20$. (*c*) Paraboloidal mirror, with real point object placed at infinite and image at $z_i = -60$.

surface $\mathcal{D}$, if and only if points A and A' are rigorously stigmatic points of the refracting surface $\mathcal{D}$. This observation is important to later develop a formal theory of geometric aberrations as a deviation of these conditions, for a point source that is outside the aplanatic points.

(b) Reflective surface

The reflective surfaces in optical imaging systems have certain advantages, such as no chromatic aberrations and the facility to design shorter systems. Therefore, it is important to manage both refractive optical surfaces and reflective optical surfaces using the same formalism.

In our expression, both the refractive surfaces and the reflective ones appear in a unified way using expression (3.7), where it is only necessary to change $n_i = -n_o$ to adapt all the formalism to the case of rigorous stigmatism by reflection. Thus, applying this condition, we write expressions (3.3)–(3.6) as

$$K = -\left(\frac{z_o - z_i}{z_i + z_o}\right)^2, \tag{5.5}$$

$$c_0 = \frac{z_i + z_o}{2 z_i z_o}, \tag{5.6}$$

$$c_1 = 0 \tag{5.7}$$

and

$$b_1 = 0. \tag{5.8}$$

Using the above quantities, expression (3.7) is reduced to equation (5.2) that represents degenerated RSS. This means that all curves representing reflective RSS are conics surfaces, which solutions for ρ is given by

$$\rho = \frac{2\cos\varphi}{c_0(K\cos^2\varphi + 1)}, \tag{5.9}$$

or in the form of Schwarzschild equation

$$z = \frac{c_0 r^2}{1 + \sqrt{1 - (1+K)c_0{}^2 r^2}}. \tag{5.10}$$

As a particular case, if $z_o \to -\infty$ or $z_i \to \infty$, the resultant surfaces are paraboloids with $K + 1 = 0$. In figure 7, we show computational results for different RSS, cases that correspond to an ellipsoidal surface, a hyperboloidal surface and a paraboloidal surface, shown from left to right.

6. Conclusion

Using the relationship between Cartesian ovals and superconic curves, we presented an implicit expression that characterizes both refractive and reflective RSS. This leads us to four shape parameters, that are functions of the refractive indexes of the media and object and image distances. Within this formulation, we have the freedom to adopt an arbitrary combination of signs for object and image distances, so, in this way, we can get every rigorously stigmatic case of optical interfaces, including object and image either real or virtual.

From the implicit expression, we got a third-order polynomial that also represents Cartesian ovals. Applying Cardano's method to this polynomial, we obtained three explicit solutions, where only one of these solutions is optically useful and able to represent every case of RSS.

We developed an analytical method for ray-tracing through RSS based on the vector form of Snell–Descartes law and this method is implemented in a computational simulation using Python, obtaining some representation of these types of surfaces. This is the base to develop a computational tool to design rigorously stigmatic lenses and subsequently the design of optical imaging systems using these types of lenses.

Data accessibility. This article has no additional data.

Authors' contributions. A.S.-L. carried out the simulation, carried out the study and drafted the manuscript; R.T. conceived of the study, designed the study, coordinated the study and helped draft the manuscript. All authors gave final approval for publication and agree to be held accountable for the work performed therein.

Competing interests. We declare we have no competing interest.

Funding. No funding has been received for this article.

Acknowledgements. The author is grateful for the financial support from the Ministerio de Ciencia, Tecnología e Innovación de Colombia, and from the Vicerrectoría de Investigación y Extensión of the Universidad Industrial de Santander.

References

1. Southall JP. 1922 Aplanatic (or Cartesian) optical surfaces. *J. Franklin Inst.* **193**, 609–626. (doi:10.1016/S0016-0032(22)90575-7)
2. Descartes R. *Discours de la méthode pour bien conduire sa raison et chercher la vérité dans les sciences, with three appendices: La Dioptrique*.
3. Huygens C. *Traité de la lumière:*$\cdots$ chez Pierre vander Aa, marchand libraire.
4. Sharma KK. 2006 *Optics: principles and applications*. Amsterdam, The Netherlands: Elsevier.
5. Villarino MB. 2007 Decartes' Perfect Lens. (http://arxiv.org/abs/0704.1059)
6. Malacara D. 2007 *Optical shop testing*. Wiley Series in Pure and Applied Optics, vol. 59. Hoboken, NY: John Wiley & Sons.
7. Güther R. 2008 Descartes ovaloides for negative refractive indices and their aplanatic cases. *Optik-Int. J. Light Electron Opt.* **119**, 577–583. (doi:10.1016/j.ijleo.2007.02.011)
8. Luneburg R, Herzberger M. 1964 *Mathematical theory of optics*. Berkeley, CA: University of California Press.

9. Bruhat M, Maréchal A, Cabannes J. 1959 *Cours de physique pour les classes de mathématiques spéciales: Optique géométrique [Texte imprimé]/par M. Bruhat,. . .A. Maréchal,. . .; préface de J. Cabannes,. . .... I*. Masson.
10. Lieb MA, Meixner AJ. 2001 A high numerical aperture parabolic mirror as imaging device for confocal microscopy. *Opt. Express* **8**, 458–474. (doi:10.1364/OE.8.000458)
11. Lynden-Bell D. 2002 Exact optics: a unification of optical telescope design. *Mon. Not. R. Astron. Soc.* **334**, 787–796. (doi:10.1046/j.1365-8711.2002.05486.x)
12. Cabral EL, De Souza J, Hunold MC. 2004 Omnidirectional stereo vision with a hyperbolic double lobed mirror. In *Proc. of the 17th Int. Conf. on Pattern Recognition, 2004. ICPR 2004, Cambridge, UK, 23–26 August*, vol. 2, pp. 1–4. Washington, DC: IEEE Computer Society.
13. Valencia-Estrada JC, García-Marquez J, Chassagne L, Topsu S. 2017 Catadioptric interfaces for designing VLC antennae. *Appl. Opt.* **56**, 7559–7566. (doi:10.1364/AO.56.007559)
14. Kano R *et al.* 2004 SolarB X-Ray Telescope (XRT). In *The Solar-B Mission and the forefront of solar physics* (eds T Sakurai, T Sekii). Astronomical Society of the Pacific Conference Series, vol. 325, p. 15. San Francisco, CA: Astronomical Society of the Pacific.
15. Sutter JP, Alianelli L. 2017 Aberration-free aspherical lens shape for shortening the focal distance of an already convergent beam. *J. Synchrotron Radiat.* **24**, 1120–1136. (doi:10.1107/S1600577517011808)
16. Michaelis D, Schreiber P, Bräuer A. 2011 Cartesian oval representation of freeform optics in illumination systems. *Opt. Lett.* **36**, 918–920. (doi:10.1364/OL.36.000918)
17. McCloskey D, Donegan J. 2013 Planar elliptical solid immersion lens based on a Cartesian oval. *Appl. Phys. Lett.* **103**, 091101. (doi:10.1063/1.4818781)
18. Valencia-Estrada JC. 2015 *Manufactura CNC de superficies Ópticas correctoras*. PhD thesis, Centro de Investigaciones en Optica, A.C.
19. Hecht E. 1998 *Hecht optics*. Reading, MA: Addison Wesley.
20. Young T. 1807 Lectures on natural philosophy. *London* **1**, 464.
21. Mahajan VN. 1998 *Optical imaging and aberrations: ray geometrical optics*. Bellingham, WA: SPIE Press.
22. Malacara-Hernandez D, Thompson BJ. 2017 *Fundamentals and basic optical lnstruments; advanced optical instruments and techniques*. Boca Raton, FL: CRC Press.
23. Fischer RE. 2008 *Optical system design*, vol. 1, 2nd edn. New York, NY: The McGraw-Hill Companies, Inc.
24. Lerner SA. 2000 Optical design using novel aspheric surfaces. PhD thesis, University of Arizona.
25. González-Acuña RG, Chaparro-Romo HA, Gutiérrez-Vega JC. 2019 General formula to design a freeform singlet free of spherical aberration and astigmatism. *Appl. Opt.* **58**, 1010–1015. (doi:10.1364/AO.58.001010)
26. Valencia-Estrada JC, García-Márquez J. 2019 Freeform geometrical optics I: principles. *Appl. Opt.* **58**, 9455–9464. (doi:10.1364/AO.58.009455)
27. Cho S. 2016 Explicit superconic curves. *JOSA A* **33**, 1822–1830. (doi:10.1364/JOSAA.33.001822)
28. Born M, Wolf E. 2013 *Principles of optics: electromagnetic theory of propagation, interference and diffraction of light*. Amsterdam, The Netherland: Elsevier.
29. Grillon T, Valencia-Estrada C, Garcia-Márquez J, Espinoza-Garcia A, Béchadergue B. 2019 Freeform geometrical optics II: from parametric representation to CAD/CAM. *Appl. Opt.* **58**, 9465–9472. (doi:10.1364/AO.58.009465)
30. Turnbull H. 1957 *Theory of equations*. University Mathematical Texts, edition 5. Edinburgh, UK: Oliver and Boyd. Method invented by Lodovico Ferrari at the request of Cardano Hieronymus and published in 1545, in his Artis Magnae, Sive de Regulis Algebraicis, liber unus.
31. Hsueh CC, Elazhary T, Nakano M, Sasian J. 2011 Closed-form sag solutions for Cartesian oval surfaces. *J. Opt.* **40**, 168–175. (doi:10.1007/s12596-011-0050-0)
32. Valencia-Estrada JC, Bedoya-Calle AH, Malacara-Hernández D. 2013 Explicit representations of all refractive optical interfaces without spherical aberration. *JOSA A* **30**, 1814–1824. (doi:10.1364/JOSAA.30.001814)
33. Shmakov SL. 2011 A universal method of solving quartic equations. *Int. J. Pure Appl. Math.* **71**, 251–259.
34. Valencia-Estrada JC, Pereira-Ghirghi MV, Malacara-Hernández Z, Chaparro-Romo HA. 2017 Aspheric coefficients of deformation for a Cartesian oval surface. *J. Opt.* **46**, 100–107. (doi:10.1007/s12596-016-0383-9)

35. Valencia-Estrada JC, Bedoya-Calle H. 2012 Lentes asféricas ovales. In *Mexican patent application. Instituto mexicano de la propiedad industrial (IMPI)*. August 30, MX/a/2012/010025.
36. Gutiérrez CE, Huang Q. 2014 The near field refractor. *Annales de l'Institut Henri Poincare (C) Non Linear Analysis* **31**, 655–684. (doi:10.1016/j.anihpc.2013.07.001)
37. Greynolds A. 2002 Superconic and subconic surface descriptions in optical design. In *Int. Optical Design Conf. Tucson, AZ, 3–5 June*, paper IMA1. OSA Technical Digest Series. Washington, DC: Optical Society of America.
38. Chen CW, Hopkins GW. 1978 Ray tracing through funnel concentrator optics. *Appl. Opt.* **17**, 1466–1467. (doi:10.1364/AO.17.001466)
39. Welford W. 1976 VI Aplanatism and isoplanatism. In *Progress in optics*, pp. 267–292. Amsterdam, The Netherlands: Elsevier.
40. Abbe E. 1873 Beiträge zur Theorie des Mikroskops und der mikroskopischen Wahrnehmung. *Archiv für mikroskopische Anatomie* **9**, 413–418. (doi:10.1007/BF02956173)
41. Malacara-Hernández D, Malacara-Hernández Z. 2016 *Handbook of optical design*. Boca Raton, FL: CRC Press.
42. Schwarzschild K. 1905 Untersuchungen zur geometrischen optic II. *Astronomische Mitteilungen der Kniglichen Sternwarte zu Göttingen* **10**, 4–28.
43. Cardano G. 1968 *The great art: or, The rules of algebra*. Cambridge, MA: MIT Press.
44. De Greve B. 2006 Reflections and refractions in ray tracing. See http://users.skynet.be/bdegreve/writings/reflection_transmission.pdf (accessed 30 May 2013).
45. Gross H, Zügge H, Peschka M, Blechinger F. 2007 *Handbook of optical systems*. Aberration Theory and Correction of Optical Systems, vol. 3. New York, NY: John Wiley & Sons.